Thermosensitive Diblock Copolymer of Poly(*N*-isopropylacrylamide) and Poly(ethylene glycol) in Water: Polymer Preparation and Solution Behavior

Ryuhei Motokawa,[†,§] Kanae Morishita,[‡] Satoshi Koizumi,[§] Takayuki Nakahira,[⊥] and Masahiko Annaka*[,‡]

Graduate School of Science and Technology, Chiba University, Chiba 263-8522, Japan; Department of Chemistry, Kyushu University, Fukuoka 812-8581, Japan; Advanced Science Research Center, JAERI, Ibaraki 319-1195, Japan; and Department of Chemistry and Biotechnology, Chiba University, Chiba 263-8522, Japan

Received December 20, 2004; Revised Manuscript Received March 26, 2005

ABSTRACT: This investigation focused on the self-assembly of poly(*N*-isopropylacrylamide)-*block*-poly(ethylene glycol) (PNIPA-*block*-PEG) in water. A quasi-living radical polymerization technique including a Ce(IV) ion redox system enabled us to prepare block copolymers with relatively narrow molecular weight distributions. We distinguish five regions in the phase diagram: a transparent sol, opaque sol, transparent gel, opaque gel, and syneresis. By examining the extent of changes in the spectroscopic properties of a fluorescence probe, pyrene, as a function of block polymer concentration and/or temperature, we determined the critical association concentration as well as the partition coefficient K_v for pyrene. The spectroscopic properties indicate that the hydrophobicity around the probe starts to increase far below the demixing line of the PNIPA-*block*-PEG, a remarkable finding which suggests that even in the temperature region below the LCST temperature of a PNIPA block (∼32 °C), this block copolymer provides more space for a preferential transfer of pyrene molecules than a bulk water medium at a higher temperature. This result may be attributed to the action of water, which starts to behave as a selective solvent for PEG blocks; the PEG chains are more swollen with water than are the PNIPA chains. Dynamic light scattering measurements also indicate that contraction of the PNIPA block starts to occur around 18 °C, which is consistent with results obtained by fluorescence measurements. By employing small-angle neutron scattering, it is also confirmed that microphase separation occurs above 17 °C to form disordered micelles, which includes a range of states from (i) asymmetric swelling to (ii) micelle formation with only short-range liquidlike order. Above 30 °C, network domains are formed as a result of macrophase separation due to dehydration of PNIPA blocks. As the temperature increased up to 40 °C, the network domain is collapsed along a direction parallel to PNIPA-*block*-PEG interface, leading to increase in interfacial thickness and to macroscopic syneresis.

1. Introduction

The behavior of amphiphilic block copolymers in aqueous solutions has attracted considerable attention in recent decades. This interest is sustained by new uses for these block copolymers in gene and drug delivery systems, microreactors for chemical synthesis and catalysis, polymeric surfactants for stabilization of colloid dispersions, etc.[1−16] Block copolymers not only have colloidal behavior similar to that of low-molecular-weight surfactants but also exhibit unique molecular architecture. Their self-aggregation depends on solvent quality, concentration, and composition. Any change in temperature, ionic strength, or pH can result in selective solvent conditions under which a medium is a solvent for at least one component of a block polymer but a nonsolvent for the other block(s). Nonionic poly(ethylene glycol)-*block*-poly(propylene glycol)-*block*-poly(ethylene glycol) (Pluronic) is a typical example.[2,17−21]

Spherical aggregates (or micelles) of block copolymers are composed of a hydrophobic core and a hydrophilic corona. These spherical aggregates may interact with each other to form networks or domain structures. Polymeric micelles are composed of a hydrophobic, water-insoluble block that associates in aqueous solution plus a hydrophilic block that inhibits the precipitation of the aggregates. This inhibition is due to a repulsive elastic energy interaction between the corona chains emanating from the cores. Because of the similarity of such aggregates to micelles made from low molar mass surfactants, amphiphilic block copolymers are often referred to as "polymeric surfactants".

An interesting combination in a block copolymer is exemplified by double-hydrophilic block copolymers in which one of the hydrophilic blocks is thermoresponsive, i.e., undergoes a transition from soluble to insoluble in water.[22] When passing through the critical temperature, one of the hydrophilic blocks collapses, thus creating hydrophobic microdomains in a manner analogous to that of a polymeric surfactant. Or, should the thermal stimulus be applied in the other direction, the aggregate formed by such block copolymers dissociates. Poly(*N*-isopropylacrylamide) (PNIPA) is well-known for its thermosensitive properties, exhibiting a lower critical solution temperature (LCST) type phase behavior in water: at room temperature, PNIPA is hydrophilic and exists as individual random coil chains, while above ∼32 °C, PNIPA becomes hydrophobic and collapses into a molecular globule.

[†] Graduate School of Science and Technology, Chiba University.
[‡] Kyushu University.
[§] JAERI.
[⊥] Department of Chemistry and Biotechnology, Chiba University.
* To whom correspondence should be addressed: Fax +81-92-642-2607; e-mail annaka-scc@mbox.nc.kyushu-u.ac.jp.

10.1021/ma047393x CCC: $30.25
Published on Web 05/24/2005

Scheme 1. Preparation of PNIPA-*block*-PEG

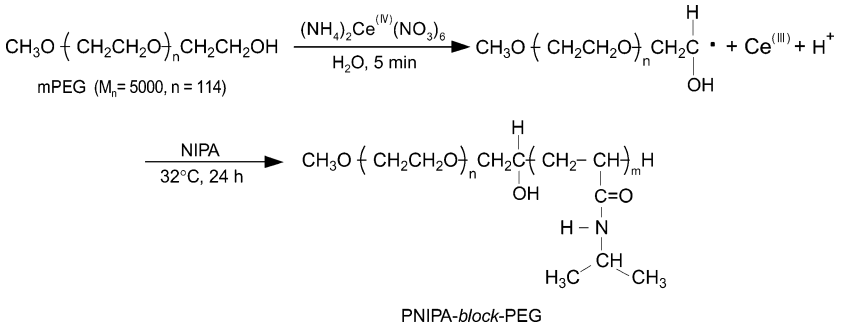

There are a number of experimental methods available for the evaluation of this self-assembly, such as the critical micelle concentration (cmc) of polymeric surfactants. Recently, fluorescence techniques have been suggested as a valuable tool for the investigation of many micelle properties.[23−27] This method can detect the onset of association for a block copolymer at a very low concentration, on the order of 1 ppm. Wilhelm et al.[28] developed the method for determining the cmc values for polystyrene-*block*-poly(ethylene glycol) in water using the fluorescence from pyrene, which is well-known as a polarity-sensitive probe. Ringsdorf et al.[29] reported thermally induced polymer conformational changes for a fluorescently labeled amphiphlic copolymer by a fluorescence technique.

In this article we report the preparation and investigation, by means of a fluorescence probe method together with dynamic light scattering, of the self-assembly, including the gelation characteristics, of poly(*N*-isopropylacrylamide)-*block*-poly(ethylene glycol) (PNIPA-*block*-PEG) in water. We also investigate the microdomain structures of aqueous solution of PNIPA-*block*-PEG by ultrasmall- and small-angle neutron scattering, which cover a wide q range from 10^{-5} to 10^{-1} Å^{-1}. Covering wide q range is crucial to elucidate a hierarchical microdomain structure formed by an aqueous solution of PNIPA-*block*-PEG.

2. Experimental Section

Materials. Monofunctional methoxy-PEG (mPEG, $\bar{M}_n$ = 5000, $\bar{M}_w/\bar{M}_n$ = 1.15, Aldrich) was purified by chromatography on activated alumina and lyophilized. NIPA monomer (kindly supplied by KOHJIN Co., Ltd.) was recrystallized from a toluene/hexane mixture and dried in vacuo. Ammonium cerium(IV) nitrate (Aldrich) was dried in an oven at 105 °C for 1 h prior to use. Reagent grade nitric acid (Kanto Chemical) was used for preparing a $(NH_4)_2Ce(NO_3)_6$ stock solution.

Instrumentation. To record ^{1}H NMR spectra**,** we used a JEOL LA-400 spectrometer operating at a frequency of 400 MHz. The sodium salt of 3-(trimethylsilyl)-1-propanesulfonic acid was used as an external standard. The probe temperature, measured with a calibrated thermocouple, was kept constant within ±0.5 °C by the passage of thermostatically regulated air during the accumulation of spectra. The molecular weight distribution of the PNIPA-*block*-PEG was estimated by gel permeation chromatography (GPC), using a TOSOH HLC-8220GPC apparatus with TSKgel $GMPW_{XL}$ × 2 and $G2500PW_{XL}$ columns, in aqueous 10 mM $NaNO_3$ solution at a flow rate of 1.0 mL/min at 10 °C. Calibration was carried out with monodisperse poly(ethylene oxide) standards purchased from TOSOH Corp.

Synthesis of PNIPA-*block*-PEG. To achieve a narrow distribution of molecular weights, we employed a soap-free emulsion polymerization; the self-organized micelle produced showed that this method worked effectively in this regard (a quasi-living radical polymerization) (Scheme 1).[32−35] A 0.1 M $(NH_4)_2Ce(NO_3)_6$ stock solution was prepared in 200 mL of 1.0 M nitric acid. Nitrogen was bubbled for 15 min through each NIPA monomer and mPEG solution prior to polymerization. In a 100 mL round-bottom flask equipped with magnetic stirrer bar, 1.0 g of mPEG was dissolved in 10 mL of distilled deionized water. To this solution, 3.3 mL of 0.1 M $(NH_4)_2Ce(NO_3)_6$ stock solution was added and stirred for 5 min, and then, x g of NIPA monomer dissolved in 12.7 mL of distilled deionized water was added. The polymerization was carried out at 32 °C for 24 h under a nitrogen atmosphere. The feed composition of the NIPA monomer is listed in Table 1. After the polymerization was completed, the solution was diluted with cold water and neutralized with a 1.0 M aqueous NaOH solution. To remove unreacted PEG, monomer, and cerium ions, we dialyzed the solution at room temperature with repeated changes of fresh distilled deionized water, followed by precipitation in hot acetone to obtain PNIPA-*block*-PEG (N_mE_n, where m and n respectively represent the number of NIPA and ethylene glycol units). In this study, we investigated three samples, coded as $N_{228}E_{114}$, $N_{143}E_{114}$, and $N_{38}E_{114}$, as summarized in Table 1.

Table 1. Feed Composition for Preparation, Molecular Weights, Molecular Weight Distributions, and Could Point (T_{tr}) of PNIPA-*block*-PEG (N_mE_n)

sample	NIPA x (g)	composition[a] m/n	$\bar{M}_n$[b]	$\bar{M}_w/\bar{M}_n$[c]	T_{tr} (°C)[d]
$N_{228}E_{114}$	1.3	228/114	30000	1.51	31
$N_{143}E_{114}$	0.88	143/114	21200	1.50	34
$N_{38}E_{114}$	0.65	38/114	9300	1.49	31

[a] Number of NIPA units (m) and ethylene glycol units (n) determined by NMR. [b] Determined by NMR. [c] Determined by GPC. [d] Determined by cloud point measurement.

Determination of Phase Diagram. The gelation and gel dissolution were examined by a vial inversion method as the temperature was increased and decreased between 5 and 45 °C at 1 °C intervals. Glass vials (1 mL) containing polymer solution samples with varying polymer concentrations were kept in a thermostated water bath for 1 h prior to their inversion. The gelation temperature was determined visually when the polymer solutions did not flow by inverting the vials. Generally, after the sample has equilibrated for 1 h, one can easily distinguish states: transparent sol, opaque sol, transparent gel, opaque gel, and syneresis.

The demixing line on the border of the transparent sol state and the opaque sol state was determined by a cloud-point measurement. Cloud points (T_{tr}) were determined by monitoring the transmittance at 500 nm of the aqueous block copolymer solution (1.0 g/L) as a function of temperature; it was recorded by a Hitachi U-3210 spectrophotometer with a temperature controlled quartz cell of 1 mm thickness. We determined T_{tr} as that corresponding to a 20% decrease in transmittance.

Fluorescence Measurements. Steady-state fluorescence spectra were recorded on a Hitachi F-4010 fluorescence spectrometer in the right-angle geometry (90° collecting optics). All spectra were run on an air−liquid equilibrated solution. Temperature control of the samples was achieved using a water-jacketed cell holder connected to a LAUDA circulating

bath. The excitation and emission slit width were set at 1.5 nm; the emission wavelength was 335 nm, and the excitation spectra were monitored at 390 nm. A typical procedure for preparing 2×10^{-6} mol/L pyrene in an aqueous solution of PNIPA-*block*-PEG is as follows: 10 μL of a 2×10^{-3} mol/L pyrene in methanol solution was added to a 10 mL volumetric flask and then dried under a mild flow of N_2 gas. After the solvent was evaporated, a calculated volume of PNIPA-*block*-PEG solution was added, diluted to 10 mL with deionized water, and stirred for 2 h.

Dynamic Light Scattering. The dynamic light scattering (DLS) experiments were conducted with a ALV CGS-8F goniometer system and a ALV DLS-5000/EPP digital correlator. The light source was a Uniphase 22 mW He−Ne laser ($\lambda = 632.8$ nm). Measurements were made at scattering angles in the range of 30−150° and at different temperatures. The time correlation functions measured by DLS were analyzed with a Laplace inversion program (CONTIN). The polymer solutions were clarified by filtering through a Millipore membrane (0.2 μm pore size). The samples were equilibrated at each measurement temperature at least for 1 h.

Small-Angle Neutron Scattering. Small-angle neutron scattering (SANS) measurements were performed at research reactor JRR-3 of JAERI (Tokai, Japan). The data were collected on the SANS-J spectrometer using a q range ($q = (4\pi/\lambda) \sin(\theta/2)$) of 3×10^{-1} Å$^{-1} \le q \le 20$ Å^{-1}. A cold neutron source was employed with wavelength $\lambda = 6.5$ Å and $\Delta\lambda/\lambda = 13\%$. The SANS measurements were carried out with D_2O solutions having polymer concentrations of 7.0, 3.0, and 0.5% for $N_{228}E_{114}$. The sample was filled in a 2 mm thick quartz cell, which typically gives a transmission of ca. 70%. The temperature was controlled to within an accuracy of 0.1 °C by circulating water. The scattered neutrons were detected by a two-dimensional position-sensitive ^{3}He detector. The data were corrected for counting efficiency, instrumental background and empty cell scattering, and radially averaged to obtain a one-dimensional data set. The scattering intensity was converted into absolute intensity units (cm^{-1}) using a secondary calibration standard of irradiated Al. Incoherent scattering from hydrogen was subtracted from the plateau value at high q.

The double-crystal spectrometer is able to cover a q region of ultrasmall-angle neutron scattering (PNO) (10^{-5} Å$^{-1} < q < 10^{-3}$ Å^{-1}) using channel-cut crystal of Si (111) and a triple bounce reflection condition. Because of the lack of luminescence of the monochromatized neutron ($\lambda = 2$ Å), a large sample size of 40 mm × 18 mm cross section and 2 mm thickness is required for a sufficient counting rate. The q profiles is obtained by PNO were corrected for background scattering and then for slit height smearing according to the infinite beam assumption. Finally, the q profiles are calibrated for absolute intensity using the calibrated q profile obtained by SANS.

3. Results and Discussion

3.1. Polymerization and Molecular Characterization. The PNIPA-*block*-PEG was prepared according to the method shown in Scheme 1. A ceric ion redox system was used to form radicals at the terminal carbons of the PEG. To prepare the block copolymer, we added a solution of ammonium cerium nitrate in 1 N nitric acid to an aqueous solution of mPEG and NIPA monomer at an initial molar ratio [Ce(IV)]/[OH end groups] of 1.2/1.0. It should be noted that PEG chains play a crucial role in starting the radical polymerization. We confirmed the role of PEG chains as we were unable to obtain PNIPA after 12 h at 34 °C when a solution of Ce(IV) was added into pure NIPA monomer solution without PEG.

Figure 1 shows the GPC chromatograms of the as-reacted sample of $N_{228}E_{114}$ and the purified $N_{228}E_{114}$ after completion of polymerization.[36] Two peaks are observed in the as-reacted sample of $N_{228}E_{114}$; the broad

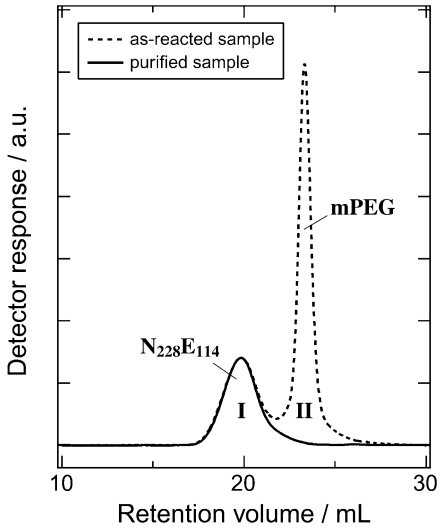

Figure 1. GPC chromatograms of the as-reacted $N_{228}E_{114}$ and the purified $N_{228}E_{114}$.

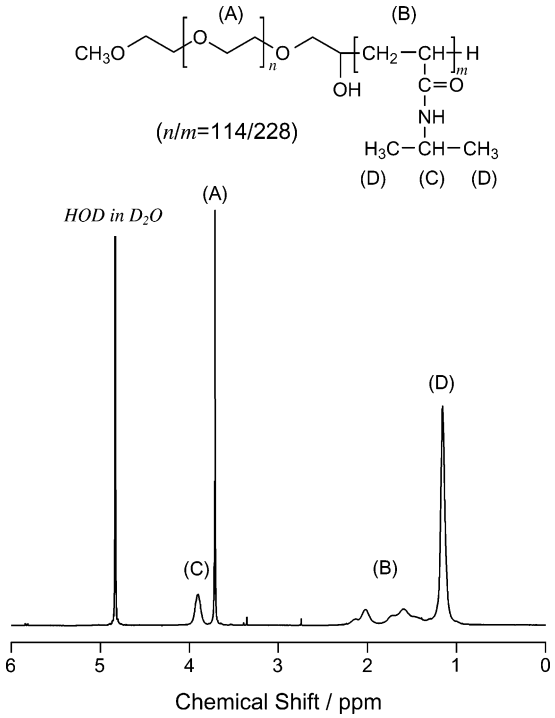

Figure 2. ^{1}H NMR spectrum of $N_{228}E_{114}$ in D_2O at 20 °C.

peak, I, with a shorter retention time, originates from the polymerized $N_{228}E_{114}$, whereas the sharp peak, II, with a longer retention time, originates from mPEG. The chromatogram of the purified sample consists of peak I only, a circumstance which enables us to characterize PNIPA-*block*-PEG precisely. The purified PNIPA-*block*-PEG has a relatively narrow molecular weight distribution (Table 1), as determined by GPC with a poly(ethylene oxide) standard calibration. The number-averaged molecular weight and the unit numbers, m and n, of N_mE_n were evaluated by comparing the area of the methylene proton peak of PEG (3.7 ppm) and methyne proton peak of PNIPA (3.9 ppm) obtained by ^{1}H NMR (Figure 2). These values are listed in Table 1.

With the addition of the NIPA monomer, the reaction mixture gradually turned from a transparent solution to a milky solution. Feijen et al.[32] reported that an

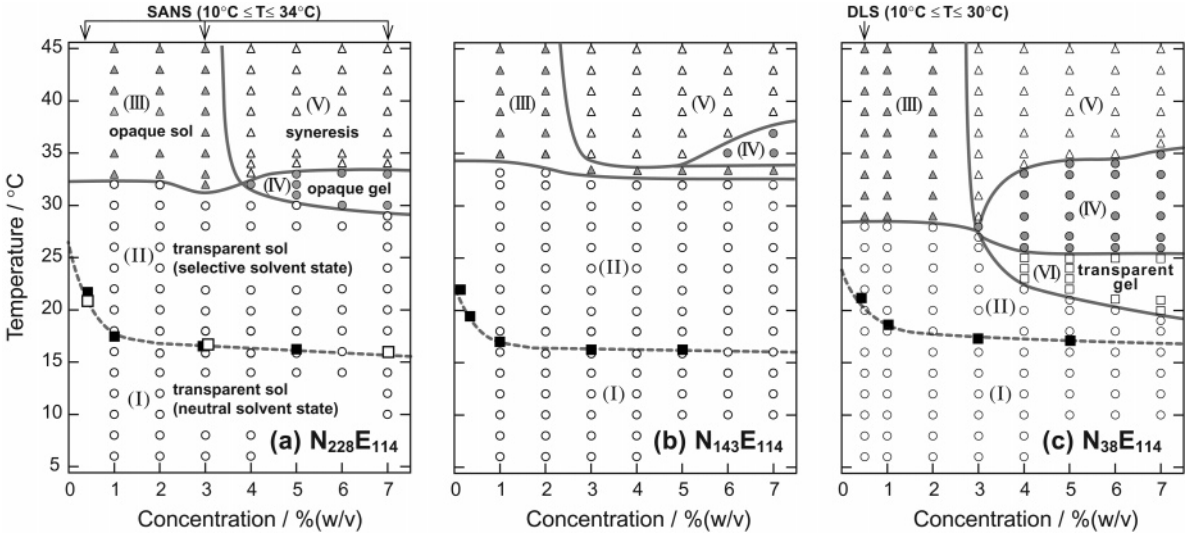

Figure 3. Phase diagrams of $N_{228}E_{114}$, $N_{143}E_{114}$, and $N_{38}E_{114}$ observed in water. (I) and (II): transparent sol; (III): opaque sol; (IV): opaque gel; (V): syneresis; region (VI): transparent gel. Regions I and II indicate the neutral and selective solvent states, respectively, determined by the onset temperature of the decrease in the I_1/I_3 value obtained from the fluorescence spectra of pyrene (solid square) and the inverse zero-angle intensity $I(0)^{-1}$ obtained from the SANS measurements (open square).

aqueous solution of a PNIPA oligomer already exhibits LCST-type thermosensitivity properties. Therefore, the observed opacity indicates the formation of micelles by the growing block copolymer. When the growing block copolymers acquire the micellization capacity, the copolymerization proceeds by a soap-free emulsion polymerization in which the NIPA monomers diffuse from the solution to the core of micelles where the propagation takes place. This type of polymerization generally yields polymers with a relatively narrow molecular weight distribution that form spherical-like micelles.

3.2. Gelation Threshold and Demixing Transition. The phase diagrams of $N_{228}E_{114}$, $N_{143}E_{114}$, and $N_{38}E_{114}$ determined in water are presented in Figure 3. As shown in Figure 3a, we distinguish macroscopically, with increases in the temperature or concentration, four regions in the phase diagram of $N_{228}E_{114}$: transparent sol (regions I and II), opaque sol (region III), opaque gel (region IV), and syneresis (region V). These changes occur reversibly, without hysteresis, when the temperature is decreased. The difference between regions I and II is discussed later with reference to the results obtained from fluorescence measurements and SANS experiments. With low block copolymer concentrations, the sample remains below the gelation threshold. A sol−gel transition is observed for a polymer concentration $C \geq 4\%$ (w/v) ($\equiv C_{gel}$: critical gelation concentration) at 33 °C. Above 34 °C, we note a syneresis, and two phases exist in solution; i.e., the polymer solution excludes the water (region V). Moreover, it is interesting to notice that for $C > C_{gel}$ the temperature needed for the onset of the demixing increases only slightly with the concentration of the block copolymers. Figure 3b shows the phase diagram of the aqueous solution of $N_{143}E_{114}$. The demixing threshold and the gelation threshold shift to a higher temperature than that in the phase behavior of the aqueous solution of $N_{228}E_{114}$. The binary mixture of $N_{38}E_{114}$ and water shows a phase behavior similar to that of the other samples except that it formed the transparent gel for $C > 3.0\%$ (w/v) and between 20 and 26 °C, shown as region VI in Figure 3c.

Taking these observations into account, we see that with increasing temperature the PNIPA chains start to collapse while the PEG chains are in a fully expanded coil state. The ^{1}H NMR spectra of purified $N_{228}E_{114}$ in D_2O at various temperatures are shown in Figure 4. The signals originate from the PNIPA chain; that peaks B−D become broader with temperature reflects the fact that the hydrophobic part tends to avoid contact with water molecules, a phenomenon which is evidence of aggregation in water at a higher temperature. The collapsed PNIPA globules may have a tendency to form hydrophobic aggregates. These aggregates of collapsed PNIPA chains form physical junctions, but they are not strong enough to hold a gel shape under the gelation threshold. Above the threshold, the PNIPA globules aggregate through hydrophobic interaction and percolate through the whole system to form the network-like

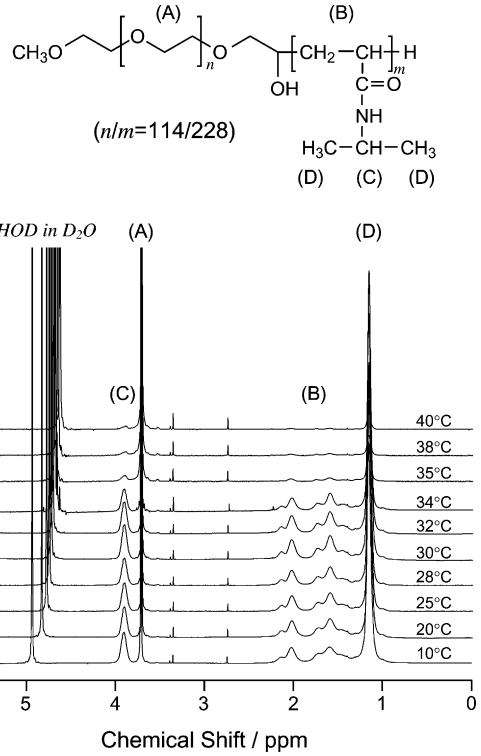

Figure 4. ^{1}H NMR spectra of $N_{228}E_{114}$ in D_2O at various temperatures.

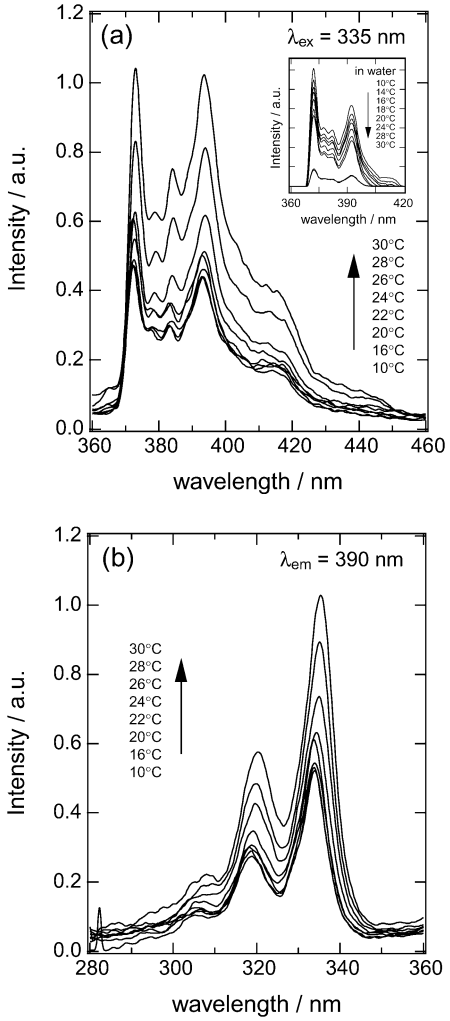

Figure 5. (a) Temperature dependence of the fluorescence spectra of pyrene (2×10^{-6} M) in 0.5% (w/v) aqueous solutions of $N_{228}E_{114}$. $\lambda_{ex} = 335$ nm. Inset: fluorescence spectra of 2×10^{-6} M aqueous solution of pyrene as a function of temperature. $\lambda_{ex} = 335$ nm. (b) Excitation spectra, monitored at $\lambda_{em} = 390$ nm, for the same sample presented in (a), showing the shift in the (0, 0) band as pyrene partitions between aqueous and micellar environments.

structure of the opaque gel. The polymer concentration effect on gel formation may be related to the degree of chain entanglement at a fixed temperature.

3.3. Self-Assembly of PNIPA-*block*-PEG in Aqueous Solutions. The self-assembly of $N_{228}E_{114}$ in aqueous solutions was examined using pyrene as a fluorescent probe. This method is based on the sensitivity of the probe to the hydrophobicity and polarity of its environment.[29,37−39] In the presence of micelles or similar supramolecular aggregates, pyrene is solubilized within the interior of the hydrophobic part (core) of such aggregates. As a result, significant changes in the spectroscopic properties are observed upon the transfer of the probe from an aqueous environment to the nonpolar environment of the core.[40] Such changes are exemplified in Figure 5, which presents typical emission and excitation data recorded for pyrene in 0.5% (w/v) aqueous solutions of $N_{228}E_{114}$ at various temperatures. The quantum yield of the fluorescence rose with temperature because the excitation state of pyrene is stabilized in the hydrophobic core and the thermal vibrational decay is suppressed. This effect was manifested by an increase in the total intensity of the

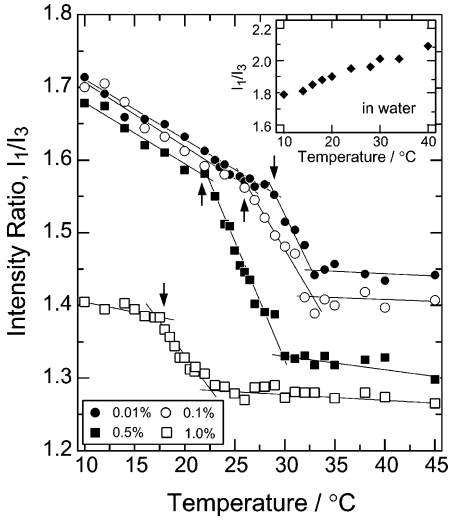

Figure 6. Changes in the ratio of intensities (I_1/I_3) of the vibrational bands in the fluorescence spectrum as a function of temperature for various concentration of $N_{228}E_{114}$. Lines are guides for the eyes. Inset: I_1/I_3 value in the fluorescence spectrum for aqueous solution of pyrene (2×10^{-6} M) as a function of temperature.

emission spectra (Figure 5a). For comparison, the fluorescence spectra for an aqueous solution of pyrene (without PNIPA-*block*-PEG) are also shown in the inset of Figure 5a. Because of the thermal deactivation, the quantum yield decreases as the temperature is raised. The vibrational fine structure of the emission spectra underwent changes. This effect was best characterized by the decrease in the ratio of I_1 ($\lambda = 373$ nm) and I_3 ($\lambda = 384$ nm) (I_1/I_3), a result which was consistent with the decrease in polarity of the environment of the pyrene. Figure 6 shows the changes in I_1/I_3 value as a function of temperature at various concentration of $N_{228}E_{114}$. As the temperature increased, the I_1/I_3 value decreased sharply in a rather narrow range of temperature and then leveled off, suggesting incorporation of the probe in the hydrophobic PNIPA domain. On the other hand, for the aqueous solution of pyrene, this ratio increases with temperature, indicating that the micropolarity experienced by the probe increases. It is worthy of note that the onset temperature of the decrease in the I_1/I_3 value is much lower than the demixing temperature of the $N_{228}E_{114}$. In the low temperature region below 16 °C, the I_1/I_3 value for 1% (w/v) $N_{228}E_{114}$ aqueous solution (open square in Figure 6) is much lower than that of the samples with a lower concentration; evidently, the $N_{228}E_{114}$ assembles to form hydrophobic domains above a particular concentration. Above the onset temperature of the decrease in the I_1/I_3 value, water may start to behave as a selective solvent for PEG blocks; the PEG chains are more swollen with water than the PNIPA chains, and such an asymmetrically swollen state might be responsible for the decrease in the I_1/I_3 value. The onset temperatures of the decrease in the I_1/I_3 value obtained from the fluorescence spectra of pyrene are plotted in Figure 3 as solid squares. Here, we see that the microphase separation is followed by this change from a neutral to a selective solvent. It should be mentioned that both the PNIPA and PEG block chains are swollen with water so that the solution is transparent, without macroscopic inhomogeneity, in this temperature region.

In the excitation spectra (Figure 5b), the increase in the fluorescence intensity with increasing temperature

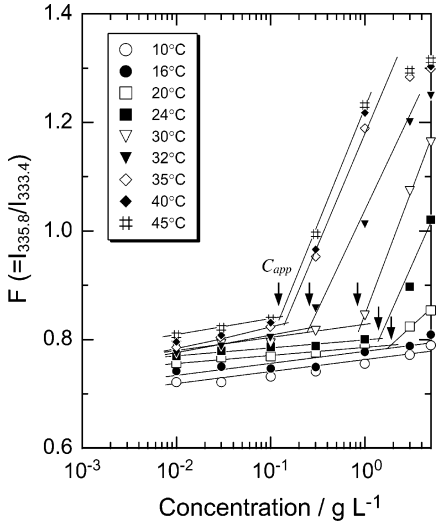

Figure 7. Plots of the intensity ratios $I_{335.8}/I_{333.4}$ (= F, from pyrene excitation spectra) as a function of $N_{228}E_{114}$ concentration. The apparent cac (C_{app}) value is taken as the intersection of the tangent to the curve at the inflection point with the horizontal tangent through the points at low polymer concentrations.

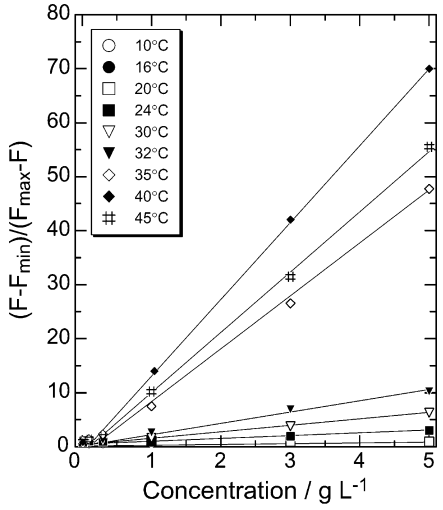

Figure 8. Plot of $(F - F_{min})/(F_{max} - F)$ as a function of $N_{228}E_{114}$ concentration at various temperatures.

results from the enhancement of the lifetime of the excited state of the pyrene. With increasing temperature, the (0,0) band in the pyrene excitation spectra, which is at 333.4 nm in water, shifted to 335.8 nm (characterized by a change of the $I_{335.8}/I_{333.4}$ intensity ratio). The dependence of this ratio with temperature is shown in Figure 7. The apparent critical association concentration (C_{app}, arrow in Figure 7) value is taken as the intersection of the tangent to the curve at the inflection with the horizontal tangent through the points at low polymer concentrations. In the concentration region below C_{app}, the magnitude of $I_{335.8}/I_{333.4}$ in Figure 7 slightly increases because the amount of the asymmetrically swollen state increases; this change, which provides more space for the preferential binding of pyrene molecules compared to the bulk water medium, is augmented by an increase in temperature.

These changes in the emission and excitation spectra are indicative of the partitioning of the pyrene between an aqueous and a hydrophobic environment. The change in the fluorescent signal can be influenced not only by the partitioning of the fluorescent probe between the aqueous and hydrophobic phases but also by the degree of polymer association.[29,39,41−43] To estimate the values of cac corresponding to the start of polymer association in these systems, we used the approach proposed by Wilhelm et al.[29] According to this method, the ratio of the pyrene concentrations (mol/L) in the hydrophobically associated polymer and water phases $[Py]_P/[Py]_W$ can be expressed as follows:

$$\frac{[Py]_P}{[Py]_W} = \frac{F - F_{min}}{F_{max} - F} \qquad (1)$$

where $F = I_{335.8}/I_{333.4}$, and F_{min} and F_{max} are the $I_{335.8}/I_{333.4}$ values determined at the zero polymer concentration and at the saturating polymer concentration, respectively. The pyrene binding to the hydrophobic phases formed from the association of PNIPA was taken to be a simple partition equilibrium between the hydrophobic phase and the water phase. Using this model, we can recalculate and linearize the data from the fluorescence spectra utilizing the following equations:

$$\frac{[Py]_P}{[Py]_W} = \frac{K_v \omega_{NIPA} c}{1000 \rho_{NIPA}} \quad \text{below cac} \qquad (2)$$

or

$$\frac{[Py]_P}{[Py]_W} = \frac{K_v \omega_{NIPA} (c - \text{cac})^2}{1000 \rho_{NIPA}} \quad \text{above cac} \qquad (3)$$

where K_v is the equilibrium constant for the partitioning of pyrene between the aqueous and PNIPA phases. c is the total concentration of PNIPA-*block*-PEG in g/L, ω_{NIPA} is the weight fraction of NIPA in the block copolymer, and ρ_{NIPA} is the density of the PNIPA core in the hydrophobic phase. The variable ρ_{NIPA} is assumed to have the same value as that of bulk NIPA, 1.1 g/mL, and not to change within the temperature range studied here, although the PNIPA core may not have been in a completely dehydrated state.[44]

Figure 8 shows the plots of the $(F - F_{min})/(F_{max} - F)$ determined from fluorescence excitation spectra obtained from various concentrations of the block copolymer. When these data are plotted according to eqs 1−3, they can be fitted to two intersecting straight lines. At high concentrations (upper plot), the slope of the line is $(K_v \omega_{NIPA}/1000 \rho_{NIPA})$, from which K_v can be calculated. Below the cac, one would expect $(F - F_{min})$ to be zero if there were no tendency of pyrene to bind to the isolated $N_{228}E_{114}$. However, the low but finite values of $(F - F_{min})/(F_{max} - F)$ at this range of polymer concentrations suggest that there is a small contribution to the pyrene signal originating in the association that develops between pyrene and the $N_{228}E_{114}$ or preaggregates. If this is the case, then the cac can be identified as the extrapolated intercept with the c-axis of the line with slope $(K_v \omega_{NIPA}/1000 \rho_{NIPA})$. Figure 9 indicates equilibrium constants, K_v, for the partitioning of the pyrene between the aqueous and PNIPA phases plotted against the solution temperature for $N_{228}E_{114}$ and $N_{38}E_{114}$. The equilibrium constant, K_v, increases sharply in a rather narrow range of temperature, a result suggesting incorporation of the probe in the hydrophobic PNIPA domain, dispersed in the matrix composed of the swollen PEG chains that were formed by the thermally induced

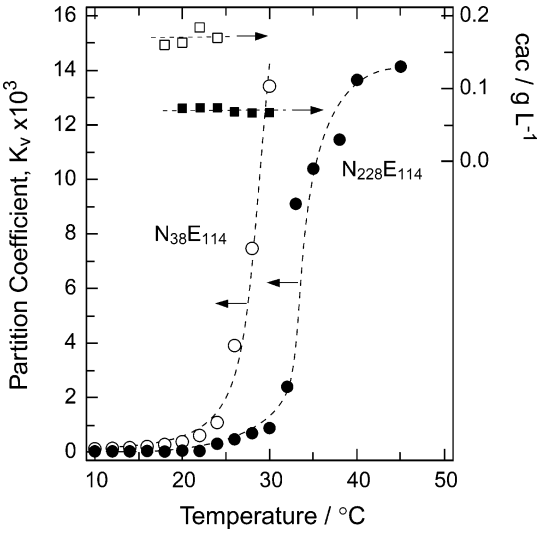

Figure 9. Equilibrium constants, K_v, for the partitioning of pyrene between aqueous and PNIPA phases (closed symbol) and cac values (open symbol) against solution temperature for $N_{228}E_{114}$ (solid symbol) and $N_{38}E_{114}$ (open symbol). Lines are guides for the eyes.

coil-to-globule transition of the PNIPA. Notably, the equilibrium constants, K_v, start to increase around 18 °C, and the K_v for the $N_{38}E_{114}$ solution is larger than that for the $N_{228}E_{114}$ solution within the temperature region studied here. These results indicate that the water may start to behave as a selective solvent for the PEG blocks, a process which leads to the formation of the PNIPA domain in the PNIPA-*block*-PEG solution.

Figure 9 also indicates the critical association concentration, cac, determined by fitting the $F = I_{335.8}/I_{333.4}$ data for PNIPA-*block*-PEG to eq 3. For both the $N_{38}E_{114}$ solution and the $N_{228}E_{114}$ solution, the cac is smaller than C_{app}, which suggests that C_{app} determined from excitation spectra provides only an estimated upper bound to cac.[29] As Wilhelm et al. pointed out, cac values determined by this method are very sensitive to the concentration regime under which the experiments are performed. In future experiments, it will be important to focus on this point to determine accurate cac values.

3.4. Dynamic Light Scattering. To investigate the temperature dependence of the characteristic dimension of PNIPA-*block*-PEG in water, we performed a DLS experiment. Measurements were made at different angles in the range of 30°−150° and at different temperatures. Figure 10a shows representative normalized intensity correlation functions $g^{(2)}(\tau)$ measured at 90° of a 0.5% (w/v) aqueous solution of $N_{38}E_{114}$ as a function of temperature. All of these functions exhibit a single relaxation corresponding to the translational diffusion of $N_{38}E_{114}$ chains. The obtained $g^{(2)}(\tau)$ was analyzed in terms of a continuous distribution of relaxation times:[45]

$$g^{(1)}(\tau) = \int_0^{+\infty} G(\Gamma) \exp(-\Gamma\tau)\, d\Gamma \qquad (4)$$

Here, $g^{(1)}(\tau)$ is the normalized electric field correlation function related to $g^{(2)}(\tau)$ via the Siegert relation. The distribution of relaxation rates was obtained by an inverse Laplace transformation of eq 4 with the CONTIN program.[46] Figure 10b shows the relaxation time distribution, $G(\Gamma)$, and relaxation rate Γ for a 0.5% (w/v) aqueous solution of $N_{38}E_{114}$ as a function of

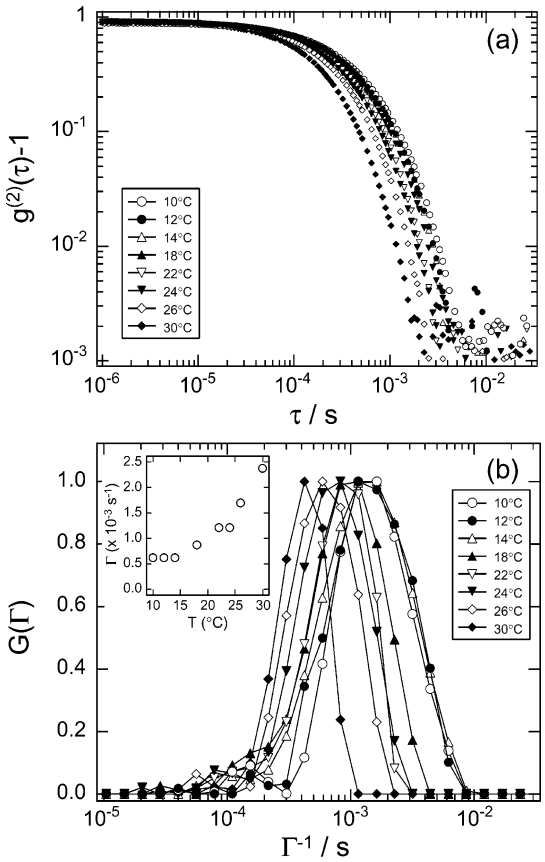

Figure 10. (a) Normalized intensity correlation functions and (b) relaxation time distribution of 0.5% (w/v) aqueous solution of $N_{38}E_{114}$ at various temperatures.

temperature. Below 18 °C, all the distribution functions at a given temperature are roughly superimposed, although some deviations are apparent. However, above 18 °C, the characteristic decay time, Γ^{-1}, shifted toward shorter relaxation times. A diffusion coefficient, D, was calculated from the position of peak as $D = \Gamma/q^2$. A selection of angular dependence of the relaxation rate is presented in Figure 11a. The selection shows linear dependence according to $\Gamma = Dq^2$ as expected for the diffusive mode. Hydrodymanic radius, R_h, was calculated using the Stokes−Einstein equation

$$R_h = \frac{k_B T}{6\pi\eta D}$$

where k_BT is the thermal energy factor, η is the temperature-dependent viscosity of solvent, and D is the diffusion coefficient. The effect of temperature on the characteristic dimension of $N_{38}E_{114}$ in water is presented in Figure 11b, and the R_h is found to decreases with increasing temperature. This difference is not due to a decrease in the solvent viscosity with increasing temperature. Since a PEG chain is a hydrophilic polymer and swells in water over a wide range of temperature, these results indicate that the contraction of PNIPA block starts to occur around 18 °C. These results are consistent with those obtained by fluorescence measurements.

3.5. Small-Angle Neutron Scattering. Figure 12 shows the SANS profiles for a 7% aqueous solution of $N_{228}E_{114}$ in the temperature range between 10 and 34 °C.[47] Below 15 °C, at a point corresponding to the transparent sol state, we obtained small-angle scatter-

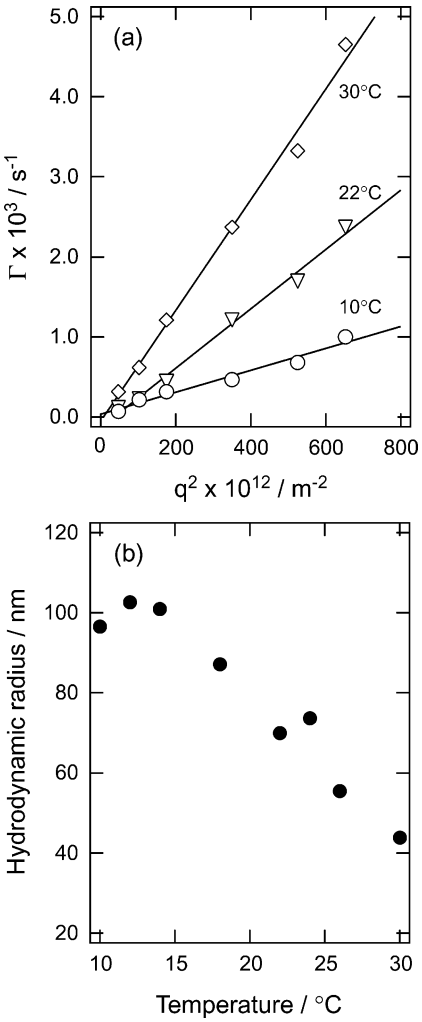

Figure 11. (a) Relaxation rate, Γ, of $N_{38}E_{114}$ at selected temperatures as a function of q^2 at selected temperatures and (b) temperature dependence of hydrodynamic radius, R_h, of $N_{38}E_{114}$.

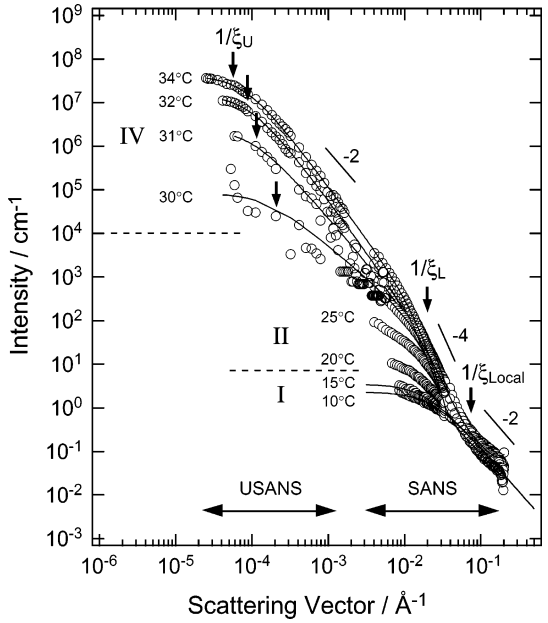

Figure 12. SANS profile obtained for 7.0% (w/v) aqueous solution of $N_{228}E_{114}$ in D_2O at various temperatures.

ing due to the thermal concentration fluctuation from the $N_{228}E_{114}$ solution in D_2O. At low q of $q\xi_{OZ} < 1$, the

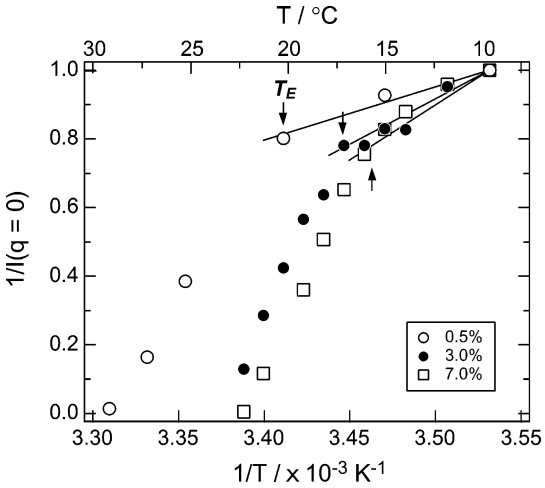

Figure 13. Plot of inverse forward scattering intensity, $1/I(0)$, vs reciprocal absolute temperature, $1/T$, for 0.5% (w/v), 3.0% (w/v), and 7.0% (w/v) aqueous solutions of $N_{228}E_{114}$ in D_2O.

SANS profile is well reproduced by the Ornstein–Zernike (OZ) type scattering function:

$$I(q) = \frac{I(0)}{1 + q^2 \xi_{OZ}^2} \tag{5}$$

where ξ_{OZ} is the thermal correlation length for the fluctuation, and $I(0)$ is the forward scattering intensity, which is determined by the osmotic compressibility. The solid lines for 10 and 15 °C in Figure 12 indicate the best-fitted scattering curves to the experimental scattering profiles by eq 5. For the length scale where $q\xi_{OZ} > 1$, $I(q)$ obeys the power law

$$I(q) \sim q^{-\alpha} \tag{6}$$

In the temperature region below 15 °C, we obtained an exponent $\alpha \cong 5/3$, indicating that both the block chains of PEG and of PNIPA swell in D_2O. The mass fractal dimension of 5/3 is due to the excluded-volume effect.

In the temperature range 17 °C $\leq T \leq$ 25 °C, $I(q)$ deviates from the OZ formalism; it exhibits a steeper q dependence or excess scattering at $q \leq 0.05$ Å^{-1}. At higher q values of $q \geq 0.05$ Å^{-1}, on the other hand, we observed the asymptotic q behavior close to $\alpha \cong 2$, indicative of the PNIPA chains being in Θ state.

To investigate the temperature dependence of the SANS profiles, we estimated the forward scattering intensity $I(0)$ with another Ornstein–Zernicke plot, where $I(0)$ was now plotted as a function of q^2. Figure 13 shows $1/I(0)$ as a function of the reciprocal absolute temperature, $1/T$. For each polymer concentration in the transparent sol region, a change in the slope of the plot of $1/I(0)$ against $1/T$ is observed around the temperature, T_E, at a crossing of two slopes. The value of T_E, thus determined, shows a coincidence with the boundary found by fluorescence measurements (open squares in Figure 3a). Above T_E, the system enters into region II.

The excess small-angle scattering observed in region II may be attributed to formation of disordered micelles, which includes a range of states from (i) asymmetric swelling to (ii) micelle formation with only short-range liquidlike order. In region II, when the temperature is raised, water gradually becomes a poor solvent for a PNIPA block, which leads to $\chi_{NW} > \chi_{EW}$, where χ_{NW} and

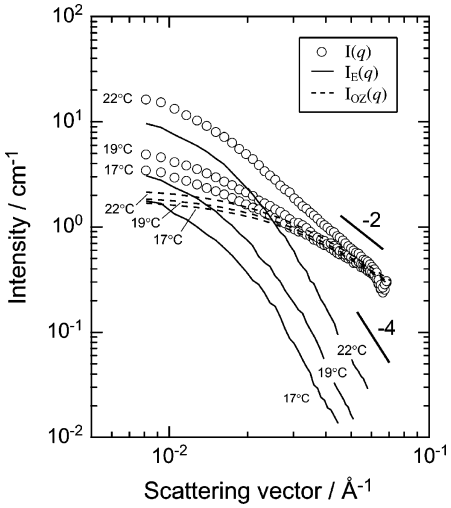

Figure 14. SANS intensity profiles and reconstructed spectra for 7% (w/v) aqueous solution of $N_{228}E_{114}$ at selected temperatures. The broken curves represent the contributions of the thermal fluctuation $I_{OZ}(q)$, the solid curves are those of excess scattering $I_E(q)$, and the full curve is total intensity.

Table 2. Correlation Lengths ξ_{OZ} and ξ_E of 7% (w/v) Aqueous Solution of $N_{228}E_{114}$ in Regions I and II Determined by SANS

temp/°C	17	18	19	20	22
ξ_{OZ}/Å	33	34	34	36	36
ξ_E/Å	70	64	64	63	63

χ_{EW} respectively indicate the Flory segmental interaction parameters between NIPA and water and between ethylene glycol and water. The micelles having scattering contrast between the poorly swollen PNIPA, and the swollen PEG may be responsible for the observed excess scattering. The micelles thus formed should have short-range liquidlike order because the solution is still in a transparent sol state. As the temperature is further increased in region II, the excess scattering becomes more pronounced and starts to show an asymptotic decay steeper than q^{-2}, which implies that micelles become a distinct structural entity with well-defined interface. Both association number of block chains in a micelle and the number of micelles are expected to increase.

The SANS q profiles are decomposed into two components of $I_{OZ}(q)$, and the excess scattering $I_E(q)$ originates from micelles with short-range order in region II; i.e., total scattering $I(q)$ is shown as a sum: $I(q) = I_{OZ}(q) + I_E(q)$. The decomposed profiles are shown in Figure 14. The asymptotic behavior of $I(q) \sim q^{-4}$ is consistent with the formation of micelles of PNIPA chains in the matrix of PEG chains. It should be mentioned that there exist no characteristic scattering maxima due to inter- or intra-microdomain scattering; therefore, the micelles are considered to have a short-range liquidlike order.

To discuss $I_E(q)$ quantitatively, a Debye−Bueche scattering function is employed:

$$I_E(q) \sim {\xi_E}^3 \left(\frac{1}{1+q^2{\xi_E}^2}\right)^2 \tag{7}$$

where ξ_E is the correlation length related to size and volume fraction of micelles. The estimated correlation lengths ξ_{OZ} and ξ_E are summarized in Table 2.

In the temperature range above 30 °C, a remarkable increase in scattering intensity was observed in the USANS region of $q < 0.001$ Å^{-1}. The q behavior in this region obeys the power law described by eq 2 with $\alpha \cong 2$. In the SANS q range, the asymptotic behavior of $I(q)$ in the region of $1/\xi_L < q < 1/\xi_{Local}$ shows the q dependence slightly steeper than q^{-4} as shown in Figure 12, which indicates that there exist a slight diffuse concentration gradient across micelle interface. ξ_L and ξ_{Local} will be discussed later. The intensity in the USANS region is attributed to the structure occurring in the larger length scale, i.e., percolated macrodomains of $N_{228}E_{114}$ in the water-rich domain. They are spatially arranged with the mass fractal dimension larger than or equal to 2.

Above 30 °C in region IV, crossovers of asymptotic q behavior are clearly seen at $q = \xi_U$, ξ_L, and ξ_{Local}, as indicated by arrows in Figure 12. These characteristic lengths represent a hierarchical structure formed by $N_{228}E_{114}$. The values ξ_U and ξ_L are considered to be upper and lower cutoff lengths of mass fractal of the macrodomains, respectively. In the q range larger than ξ_L, we observe the interfacial structure of macrodomains for $1/\xi_L < q < 1/\xi_{Local}$ and segmental distribution of swollen chains in the macrodomains and matrix for $1/\xi_L < q$.

To the qualitatively analyze the crossover in the asymptotic q behavior in $I(q)$ above 30 °C, we used a two-term model composed of terms account for short-range, thermal fluctuations of the chain in a semidilute solution $I_{OZ}(q)$ and longer-range contribution arising from the elastic constraint due to the networklike domain formation $I_d(q)$, i.e., $I(q) \sim I_d(q) + I_{OZ}(q)$. $I_d(q)$ is given by $I_d(q) \sim P(q)S(q)$, where $P(q)$ and $S(q)$ are a form factor and a structure factor, respectively. A squared-Lorentian function is employed for the form factor:

$$P(q) = \left(\frac{1}{1+q^2{\xi_L}^2}\right) \exp(-\sigma^2 q^2) \tag{8}$$

where σ is related to the width of the diffuse interfacial boundary.[48] An equation for silica gel particle aggregates assuming power-law correlations between particles and a finite correlation length proposed by Freltoft et al.[49] was used for the structure factor

$$S(q) = 1 + \frac{C(d_m-1)\Gamma(d_m-1)\xi_U^d}{(1+q^2{\xi_U}^2)^{d/2}} \frac{(1+q^2{\xi_U}^2)^{1/2}}{q\xi_U} \times \frac{\sin[(d_m-1)\arctan(q\xi_U)]}{d_m-1} \tag{9}$$

where d_m, Γ, and C are the mass fractal dimension ($1 < d_m < 3$), gamma function, and a proportionality constant, respectively. In eqs 8 and 9, the lower and upper cutoff lengths for mass fractal structures are considered as ξ_L and ξ_U, respectively.

The solid lines in Figure 12 are the fit to the experimental data using eqs 8 and 9 at the temperatures above 30 °C, and Table 3 gives the values for obtained parameters. As the temperature is raised, the upper cutoff length of mass fractal of the macrodomains ξ_U increases, while the lower cutoff length ξ_L is insensitive to temperature. Fractal dimension d_m increases from 1.51 to 2.39 with temperature, indicating that the macrodomains are packed more densely in space at

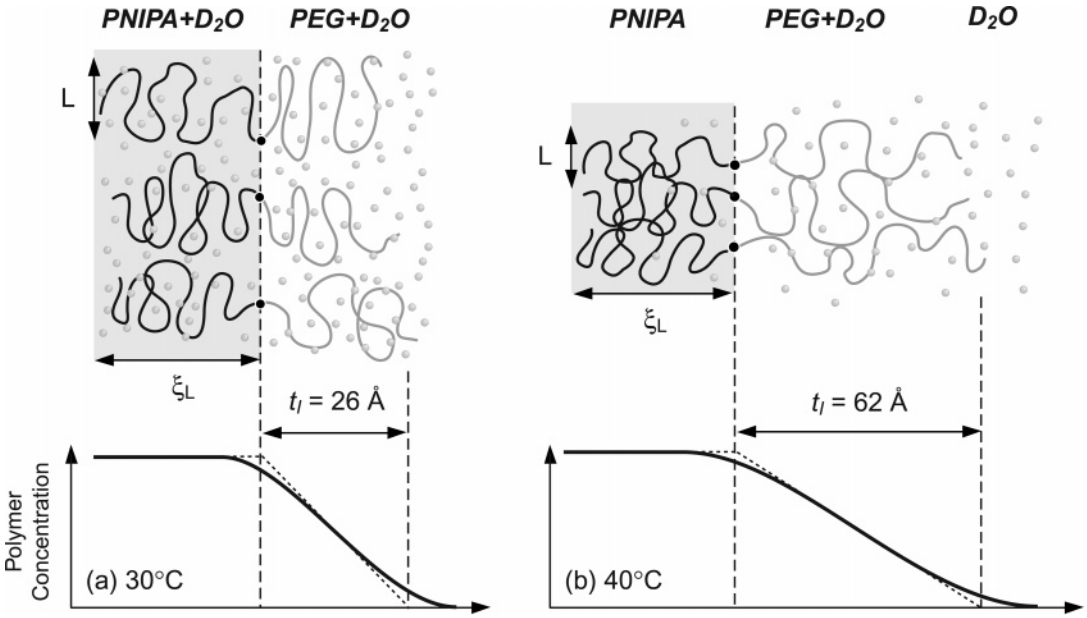

Figure 15. Schematics of interfacial structures for $N_{228}E_{114}$ in (a) opaque gel state at 30 °C and (b) syneresis state at 40 °C. Characteristic interfacial thickness t_I reflects segmental distribution of PEG chains. The values are obtained for 7% (w/v) aqueous solution of $N_{228}E_{114}$, and the dotted lines show how t_I of the diffuse interface is defined.

Table 3. Fitted Structure Parameters of 7% (w/v) Aqueous Solution of $N_{228}E_{114}$ in Regions IV and V Determined by SANS and USANS

temp/°C	ξ_L/Å	ξ_U/Å ($\times 10^3$)	d_m	σ/Å	t_I/Å
30	49	8.02	1.51	10.3	26
31	49	11.4	2.08	1.08	27
32	50	12.2	23.9	1.99	50
34	50	13.8	23.9	2.21	55
40				24.9	62

higher temperature. The parameter σ in eq 8 is related to the characteristic interfacial thickness t_I[48,50]

$$t_I = (2\pi)^{1/2}\sigma \tag{10}$$

The interfacial structure of aqueous solution is schematically shown in Figure 15, where the surface of the macrodomains is covered with PEG brushes swollen with water. It should be noted that the scattering lengths of PNIPA, b_{PNIPA} ($= 1.23 \times 10^{-14}$cm^{-2} mol), and PEG, b_{PEG} ($= 0.94 \times 10^{-14}$cm^{-2} mol), are similar and smaller than that of deuterated water, b_{D_2O} ($= 9.49 \times 10^{-14}$ cm^{-2} mol). Therefore, t_I observed by SANS corresponds to a spatial distribution of D_2O across the interface between PNIPA-rich macrodomain and swollen PEG chains. As indicated in Table 3, the characteristic interfacial thickness, t_I, becomes larger with increasing temperature. This change in t_I is probably explained by changes in packing density. Above 30 °C, the PNIPA chains of PNIPA-*block*-PEG are collapsed due to the increase in hydrophobicity. This leads to decrease in the interfacial area per chain or average length, L, between the junctions of block chains, as illustrated in Figure 15. However, the PEG chains are swollen, and this leads to a difference in the segmental volumes of PNIPA and PEG. To retain normal liquid-state densities, the PEG block must stretch as shown in Figure 15.

3.6. Morphologies and Ordering Mechanism of Phases. On the basis of the microscopic observations by fluorescence spectroscopy, DLS and SANS, we schematically present the elucidated morphologies of the system and then consider the ordering mechanism for the aqueous PNIPA-*block*-PEG solution.

In the transparent sol region I, both PNIPA and PEG blocks are swollen with water. While in region II, PNIPA-*block*-PEG forms disordered micelles in short-range liquidlike order, as shown in Figure 16b where the micelles are comprised of PNIPA cores and PEG brushes. Near the boundary between regions I and II, unimolecular micelles might be formed as a consequence of the asymmetric swelling of PNIPA and PEG block chains (Figure 16a).

The opaque sol observed in region VI is attributed to the network composed of the percolated PNIPA-rich domains coexisting with PEG-rich domains. PNIPA domains are less swollen with water than PEG domains (Figure 16c). In the opaque sol region III, on the other hand, we could not observe the gel state at higher temperatures, which indicates that PNIPA-rich domains are not percolated into whole system (Figure 16d). The characteristic length ξ_L, therefore, corresponds to that of PNIPA-rich domain, as indicated in Figure 16c,d. The network in the region IV has the mass fractal structure with fractal dimension $d_m \cong 1.5-2.4$ in the length scale limited by ξ_L and ξ_U. The increase in d_m with temperature is due to that in the packing density of PNIPA domains.

The characteristic length ξ_L, related to the size of PNIPA-rich domain, is insensitive to temperature in region IV. This may be a result of a competitive balance between a dehydration of PNIPA domains that acts to shrink ξ_L and stretching of PEG chains in PEG domains that acts to expand ξ_L, as illustrated in Figure 15. As the temperature is further increased into region V, water is squeezed out from the gel phase that is caused by contraction of PNIPA chains.

The ordering of aqueous solution of PNIPA-*block*-PEG is likely to proceed by two steps: i.e., (i) microphase separation between PNIPA and PEG block chains and (ii) macrophase separation between PNIPA-*block*-PEG and water. PNIPA-*block*-PEG solution is a ternary system of PNIPA block, PEG block, and water; therefore, three interaction parameters, χ_{NE}, χ_{NW}, and χ_{EW},

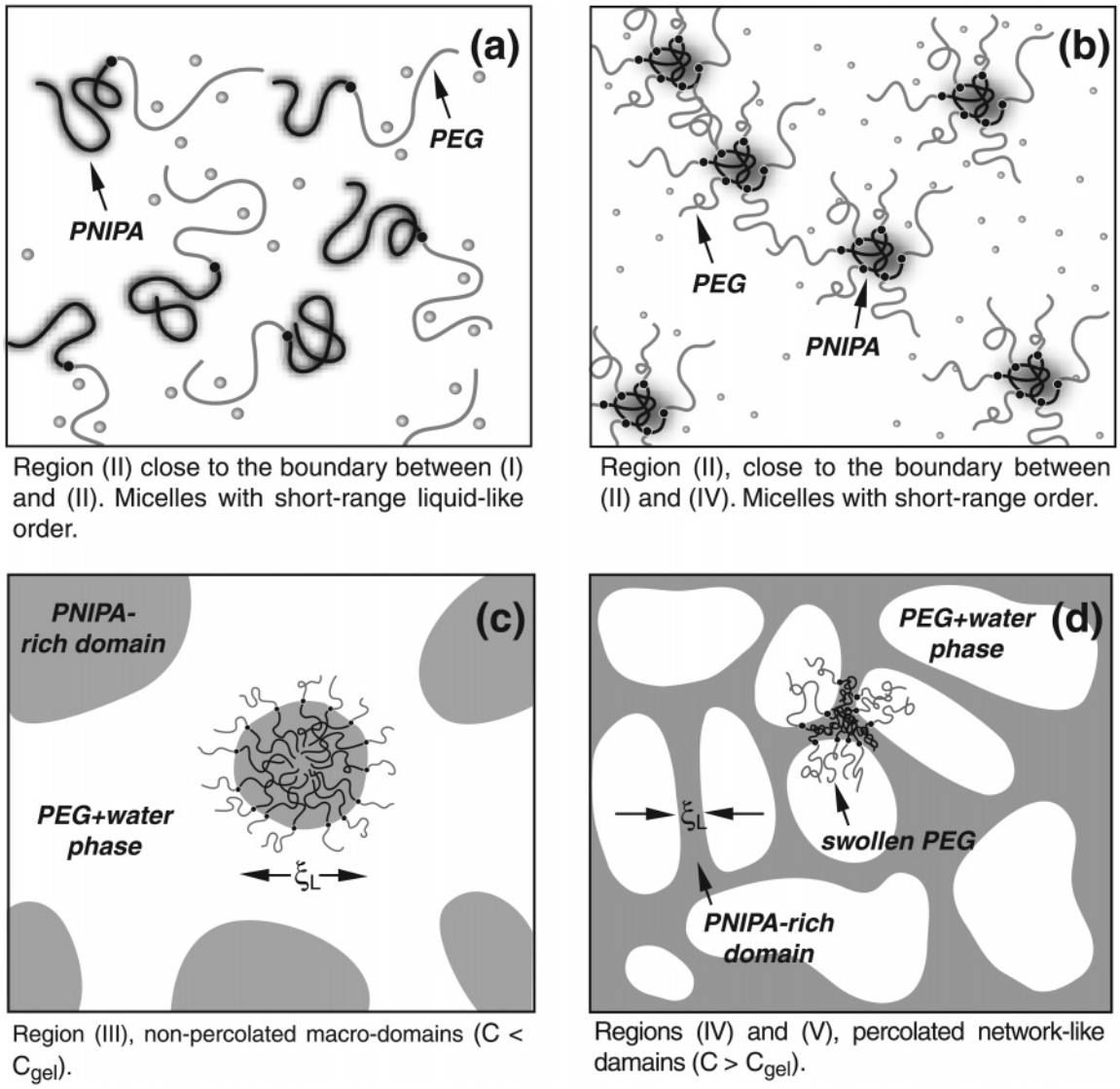

Region (II) close to the boundary between (I) and (II). Micelles with short-range liquid-like order.

Region (II), close to the boundary between (II) and (IV). Micelles with short-range order.

Region (III), non-percolated macro-domains ($C < C_{gel}$).

Regions (IV) and (V), percolated network-like damains ($C > C_{gel}$).

Figure 16. Schematic illustrations of micellar and networklike structures for 7.0% (w/v) aqueous solutions of $N_{228}E_{114}$ in D_2O proposed by SANS and USANS.

determine the thermodynamic instabilities of macro- and microphase separations.

In region I, both block chains of PNIPA and PEG are swollen with water. According to the dilution approximation,[51] interaction between PNIPA and PEG chains are weakened into $\phi\chi_{NE}$ and a disordered state is stabilized by swelling. When the temperature is increased into region II, solvent selectivity, $\Delta\chi$ ($= \chi_{NW} - \chi_{EW}$), becomes larger. A change in $\Delta\chi$ also contributes to the interaction between PNIPA and PEG block chains. As a result of two competitive contributions of dilution approximation and solvent selectivity, PNIPA-*block*-PEG starts to form micelles in region II.

Within the framework of mean-field approximation, macrophase separation between PNIPA-*block*-PEG and water is determined by the χ parameter, which is averaged for two block chains as $\chi_{macro} = f_{PNIPA}\chi_{NW} + (1 - f_{PNIPA})\chi_{EW}$, where f_{PNIPA} is the volume fraction of PNIPA. In the temperature range studied here, water behaves as a good solvent for PEG chains; therefore, χ_{macro} can be approximated to $\chi_{macro} = f_{PNIPA}\chi_{NW}$. Using this assumption, we obtain $\chi_{macro} \cong 0.83\chi_{NW}$ for $N_{228}E_{114}$ and $\chi_{macro} \cong 0.46\chi_{NW}$ for $N_{38}E_{114}$. The macrophase separation for $N_{38}E_{114}$ is suppressed compared to $N_{228}E_{114}$, which provides the qualitative explanation that $N_{38}E_{114}$ exhibits the transparent gel state in region IV. On further increase in temperature, χ_{macro} satisfies the condition for macrophase separation above 30 °C, which determines the phase boundary between regions II and III for $N_{228}E_{114}$ and $N_{143}E_{114}$ and between regions VI and VI for $N_{38}E_{114}$. The opaque sol observed in region III corresponds to macrophase separation, where micelles are dispersed in water.

In region IV, we observed the networklike domain with mass fractal structure exhibits power low scattering ($\sim q^2$) for the q region of $1/\xi_U < q < 1/\xi_L$. This networklike domain is likely to have a morphology characteristic for "viscoelastic phase separation".[52−55] A mechanism to form such a network may be regarded as diffusion-limited association (DLA) of micelles; the micelles diffuse and aggregate to minimize an interfacial area with temperature. In the DLA process, dynamical asymmetry between micelles and water is also an important factor; here the term "asymmetry" denotes the difference in mobility. It is well established that the dynamical asymmetry induces local stress imbalance between fast and slow components and affects phase separation and relaxation of concentration fluctuation

in order to transiently release stress imbalance during the ordering process (dynamical coupling between stress and diffusion). In the system studied here, micelles formed by PNIPA-*block*-PEG and water correspond to slower and faster components, respectively. The dynamical coupling in the DLA process involves the association of the micelles into the networklike domain in water. If the reorganization of domain structures is allowed, the networklike domains should be transformed into clusters of droplets, in hydrodynamic limits, to reduce the interfacial free energy. Aqueous solution of PNIPA-*block*-PEG, however, exhibits a distinct behavior in this sense; SANS measurement confirmed the networklike structure remains in region V. This pinning of the domain growth is probably caused by aggregation and vitrification of PNIPA chains.

The compound PNIPA is known to be a thermosensitive polymer, and the combination of the dehydration of the chains and the entropic force of the chains induces the coil-to-globule transition.[56] The dehydration is induced by the destabilization of the clustered water molecules surrounding the isopropyl group when their chemical potential exceeds that of bulk water. The coil-to-globule transition of PNIPA achieved by adding salt[57,58] or saccharide[59] has also been explained by the dehydration mechanism. Since PNIPA exhibits only a small change in chain dimension at lower temperatures in water,[60] the observed change in the solvent selectivity around 18 °C, which is far below the LCST temperature of the PNIPA block (∼32 °C), may be related to the unique architecture of PNIPA-*block*-PEG. The connection of the hydrophilic PEG block to the PNIPA block is thought to reduce the chemical potential of water molecules to destabilize the hydrated state of PNIPA chains, resulting in a decrease in the transition temperature.[61] Because of the higher PEG content of $N_{38}E_{114}$ as compared with $N_{228}E_{114}$, the hydrated state of PNIPA chains of $N_{38}E_{114}$ is less stable than that of $N_{228}E_{114}$, a siutation which is responsible for the formation of the PNIPA domain in the aqueous solution of $N_{38}E_{114}$ at a lower temperature. This phenomenon leads the aqueous solution of $N_{38}E_{114}$ to have a higher K_v value.

4. Concluding Remarks

We have studied the self-assembly behavior of aqueous solution of PNIPA-*block*-PEG prepared by the quasiliving radical polymerization technique using a ceric ion redox system. For the aqueous PNIPA-*block*-PEG solution, we macroscopically distinguish, with changes in the temperature and/or concentration, five regions in the phase diagram: transparent sol, opaque sol, transparent gel, opaque gel, and syneresis. Because of the dehydration of the PNIPA block above 32 °C, a macrophase separation in the aqueous solution of PNIPA-*block*-PEG occurs to form PNIPA-rich domains dispersed in the matrix composed of the swollen PEG chains and water.

When traces of pyrene are added to $N_{228}E_{114}$ aqueous solutions, the pyrene partitions into the hydrophobic core phase. Several aspects of its spectroscopic properties are changed upon transfer into the more hydrophobic environment. The (0,0) band is shifted from 333.4 to 335.8 nm in the hydrophobic core. The vibrational fine structure (the I_1/I_3 ratio) undergoes the changes expected for this kind of transfer. By examining the extent of these changes as a function of block polymer concentration and/or temperature, we can identify and determine the critical association concentration to be on the order of 0.3−0.8 g/L and determine as well the partition coefficient K_v for pyrene, ranging from about 10^2 to 10^3. Remarkably, the spectroscopic properties indicate that the hydrophobicity around the probe starts to increase around 17 °C, a level which is far below the LCST temperature of the PNIPA block (∼32 °C) of the PNIPA-*block*-PEG. Evidently, the PNIPA-*block*-PEG, compared to the bulk water, starts to provide space for a preferential transfer of the pyrene molecules. It is likely that water behaves as a selective solvent for PEG blocks; the PEG chains are more swollen with water than are the PNIPA chains. Our DLS measurements also indicate that the contraction of the PNIPA block starts to occur around 18 °C. Such an asymmetrically swollen state might be responsible for the observed spectroscopic properties. It should be noted that in this temperature region both the block chains of the PNIPA and the PEG are swollen with water, so that the solution is transparent, without macroscopic inhomogeneity. The temperatures at which water starts to become a selective solvent for PEG blocks determined by the fluorescence and DLS measurements are consistent with those determined by SANS.

The microstructures of PNIPA-*block*-PEG in water were also investigated by SANS measurements over a wide q range from 10^{-5} to 10^{-1} Å^{-1}. Microphase separation occurs above 17 °C, where $I(q)$ deviates from the OZ formalism in that it shows a steeper q behavior or excess scattering in the low q region resulting from the formation of disordered micelles, which includes a range of state from asymmetric swelling and micelle with short-range liquidlike order. Above 30 °C, network domains are formed as a result of macrophase separation due to dehydration of PNIPA blocks. As the temperature increased up to 40 °C, the network domain is collapsed along a direction parallel to PNIPA-*block*-PEG interface, leading to increase in interfacial thickness and to macroscopic syneresis.

Acknowledgment. The work was partly supported by a Grant-in-Aid (No. 15340137) and Grant-in-Aid for Scientific Research on Priority Areas (No. 16041233) from the Ministry of Education, Culture, Sports, Science, and Technology (for M. Annaka). M.A. acknowledges the financial support from the Kurata Memorial Hitachi Science and Technology Foundation. The authors also acknowledge Mr. Fumiya Nakata, Mr. Tsutomu Ishimaru, and Mr. Kenji Sasaki of TOSOH Co. Ltd. for technical support and helpful discussions.

References and Notes

(1) Muthukumar, M.; Ober, C. K.; Thomas, E. L. *Science* **1997**, *277*, 1225.
(2) Almgren, M.; Brown, W.; Hvidt, S. *Colloid Polym. Sci.* **1995**, *272*, 2 and references therein.
(3) Forster, S.; Antonietti, M. *Adv. Mater.* **1998**, *10*, 195.
(4) Scholz, C.; Iijima, M.; Nagasaki, Y.; Kataoka, K. *Macromolecules* **1995**, *28*, 7295.
(5) Gref, R.; Minamitake, Y.; Peracchia, M. T.; Trubetskoy, V.; Torchilin, V.; Langer, R. *Science* **1994**, *263*, 1600.
(6) *Self-Assembling Complexes for Gene Delivery. From Laboratory to Clinical Trail*; Kabanov, A. V., Felgner, P., Seumour, L., Eds.; John Wiley: Chichester, 1998.
(7) Cammas, S.; Kataoka, K. In *Solvents and Self-Organization of Polymers*; Webber, S. E., Munk, P., Tuzar, Z., Eds.; Kluwer Academic Publishers: Dordrecht, The Netherlands, 1996; p 83.

(8) Alakhov, V. Yu.; Kabanov, A. V. *Expert. Op. Invest. Drugs* **1998**, *7*, 1453.
(9) Bronstein, L.; Sidorov, S.; Valetsky, P.; Hartman, J.; Colfen, H.; Antonietti, M. *Langmuir* **1999**, *15*, 6256.
(10) Bronstein, L.; Chernyshov, D.; Timofeeva, G.; Dubrovina, L.; Valetsky, P.; Obolonkova, E.; Khokhlov, A. *Langmuir* **2000**, *16*, 3626.
(11) Wang, G.; Hanselwood, F.; Liu, G. *Langmuir* **1998**, *14*, 1554.
(12) Greutz, S.; Jerome, R. *Langmuir* **1999**, *15*, 7145.
(13) Urban, D.; Gerst, M.; Rossmanith, P.; Schuch, H. *Polym. Mater. Sci. Eng.* **1998**, *79*, 4023.
(14) Yokoyama, M.; Kwon, G. S.; Okano, T.; Sakurai, Y.; Seto, T.; Kataoka, K. *Bioconjugate Chem.* **1992**, *3*, 295.
(15) Kwon, G. S.; Kataoka, K. *Adv. Drug Delivery Rev.* **1995**, *16*, 295.
(16) *Biorelated Polymers and Gels. Controlled Release and Applications in Biomedical Engineering*; Okano, T., Ed.; Academic Press: Boston, 1998.
(17) Tuzar, Z.; Kratochvil, P. Micelles of Block and Graft Copolymers in Solutions. In *Surface and Colloid Science;* Matijevic, E., Ed.; Plenum: New York, 1993; Vol. 15, p 1.
(18) Chu, B.; Zhou, Z. Physical Chemistry of Polyoxyalkylene block Copolymer Surfactants. In *Nonionic Surfactants, Polyoxyalkylene Block Copolymers*; Nace, V. N., Ed.; Marcel Dekker: New York, 1996; Vol. 60 and references therein.
(19) Hamley, I. W. *The Physics of Block Copolymers*; Oxford University Press: New York, 1998 and references therein.
(20) Wanka, G.; Hoffmann, H.; Ulbricht, W. *Macromolecules* **1994**, *27*, 4145.
(21) Zhang, K. PhD Thesis, University of Lund, 1994.
(22) Arotcarena, M.; Heise, B.; Ishaya, S.; Laschewsky, A. *J. Am. Chem. Soc.* **2002**, *124*, 3787.
(23) Vorobyoba, O.; Lau, W.; Winnik, M. A. *Langmuir* **2001**, *17*, 1357.
(24) Kalyanasundaram, K. In *Photochemistry in Microheterogeneous Systems*; Academic Press: Orlando, FL, 1987.
(25) Grieser, F.; Drummond, D. J. *J. Phys. Chem.* **1988**, *92*, 5580.
(26) Almgren, M.; Lofroth, J. E.; Van Stem, J. *J. Phys. Chem.* **1986**, *90*, 4431.
(27) Virtanen, J.; Holappa, S.; Lemmetyinen, H.; Tenhu, H. *Macromolecules* **2002**, *35*, 4763.
(28) Wilhelm, M.; Zhao, C. L.; Wang, Y.; Xu, R.; Winnik, M. A.; Mura, J.-L.; Riess, G.; Croucher, M. D. *Macromolecules* **1991**, *24*, 1033.
(29) Ringsdorf, H.; Venzmer, J.; Winnik, F. M. *Macromolecules* **1991**, *24*, 1678.
(30) Bonse, U.; Heart, M. *Appl. Phys. Lett.* **1968**, *7*, 238.
(31) Aizawa, K.; Tomimitsu, H. *Physica B* **1995**, *213*−*214*, 884.
(32) Topp, M. D. C.; Dijkstra, P. J.; Talsma, H.; Feijen, J. *Macromolecules* **1997**, *30*, 8518.
(33) Nagarajan, S.; Sabdham, K.; Srinivasan, V. *J. Polym. Sci., Part A: Polym. Chem.* **1995**, *33*, 2925.
(34) Topp, M. D. C.; Leunen, I. H.; Dijkstra, P. J.; Tauer, K.; Schellenberg, C.; Feijen, J. *Macromolecules* **2000**, *33*, 4986.
(35) Odian, G.; Kho, J. H. H. *J. Macromol. Sci., Part A: Chem.* **1970**, *4*, 317.
(36) Motokawa, R.; Nakahira, T.; Annaka, M.; Hashimoto, T.; Koizumi, S. *Polymer* **2004**, *45*, 9019.
(37) Lee, S.; Chang, Y.; Yoon, J.-S.; Kim, C.; Kwon, I.; Kim, Y.-H.; Jeong, S. *Macromolecules* **1999**, *32*, 1847.
(38) Lee, A.; Gast, A.; Butun, V.; Armes, S. *Macromolecules* **1999**, *32*, 4302.
(39) Astafieva, I.; Zonng, X.; Eisenberg, A. *Macromolecules* **1993**, *26*, 7339.
(40) Kalyanasundaram, K.; Thomas, J. K. *J. Am. Chem. Soc.* **1977**, *99*, 2039.
(41) Cheon, J.-B.; Jeong, Y.-I.; Cho, C.-S. *Polymer* **1999**, *40*, 2041.
(42) Vorobyova, O.; Lau, W.; Winnik, M. A. *Langmuir* **2001**, *17*, 1357.
(43) Lysenko, E. A.; Bronich, T. K.; Slonkina, E. V.; Eisenberg, A.; Kabanov, V. A.; Kabanov, A. V. *Macromolecules* **2002**, *35*, 6351.
(44) Shirota, H.; Endo, N.; Horie, K. *Chem. Phys.* **1998**, *238*, 487.
(45) Berne, B. J.; Pecora, R. *Dynamic Light Scattering with Applications to Chemistry, Biology, and Physics*; Wiley: New York, 1976.
(46) Provencher, S. W. *Biophys. J.* **1976**, *16*, 27.
(47) Motokawa, R.; Annaka, M.; Nakahira, T.; Koizumi, S. *Colloids Surf. B* **2004**, *38*, 213.
(48) Ruland, W. *J. Appl. Crystallogr.* **1971**, *4*, 70.
(49) Freltoft, T.; Kjems, J. K.; Shinha, S. K. *Phys. Rev. B* **1986**, *33*, 269.
(50) Hashimoto, T.; Shibayama, M.; Kawai, H. *Macromolecules* **1980**, *13*, 1237.
(51) Helfand, E.; Tagami, Y. *J. Chem. Phys.* **1972**, *56*, 3592.
(52) Doi, M.; Onuki, A. *J. Phys. II* **1992**, *2*, 1631.
(53) Tanaka, H. *J. Phys: Condens. Matter* **2000**, *12*, 207.
(54) Toyoda, N.; Takenaka, M.; Saito, S.; Hashimoto, T. *Polymer* **2001**, *42*, 9193.
(55) Takenaka, M.; Takeno, H.; Hasegawa, H.; Saito, S.; Hashimoto, T.; Nagao, M. *Phys. Rev. E* **2002**, *65*, 021806-1.
(56) Sasaki, S.; Maeda, H. *Phys. Rev. E* **1996**, *54*, 2761.
(57) Park, T. G.; Hoffman, A. S. *Macromolecules* **1993**, *26*, 5045.
(58) Annaka, M.; Motokawa, K.; Sasaki, S.; Nakahira, T.; Kawasaki, H.; Maeda, H.; Amo, Y.; Tominaga, Y. *J. Chem. Phys.* **2000**, *113*, 5980.
(59) Kawasaki, H.; Sasaki, S.; Maeda, H.; Mihara, S.; Tokita, M.; Komai, T. *J. Phys. Chem.* **1996**, *100*, 16282.
(60) Wu, C.; Zhou, S. *Macromolecules* **1995**, *28*, 8381.
(61) Sasaki, S.; Kawasaki, H.; Maeda, H. *Macromolecules* **1997**, *30*, 1847.

MA047393X